

Laboratory 5:

Geometric Optics

Name: Omar Ozgur

Date: Feb 18, 2016

Lab: Section 7, Thursday 8:00am

TA: Nicholas Rombes

Lab Partner: Uday Alla

1. Introduction

The purpose of this experiment was to explore various properties of geometric optics. In the first section of the experiment, a beam of light was directed towards a trapezoidal prism at specific angles in order to determine properties such as the index of refraction of the prism, as well as the critical angle for total internal reflection. The experimental data was compared to theoretical results in order to verify Snell's Law. In the second set of experiments, a bi-convex, bi-concave, and plano-convex lens were used to analyze properties of thick lenses such as focal length, spherical aberration, and one-dimensional magnification. In the third set of experiments, the focal length was measured for various thin lenses, as well as the surface of an acrylic sphere. In the final portion of the experiment, a thin lens was used to show an image on a moveable screen based on an illuminated millimeter grid. The object distance, image distance, and image size was measured for 5 different setups, and the results were compared to theoretical values and trends. The results of these experiments helped to verify theoretical properties of geometric optics.

2. Experimental Results

2.1 Snell's Law and Total Internal Reflection

2.1.2: Snell's Law

In the first section of the experiment, the goal was to use experimental data to verify Snell's Law. Before beginning the lab, a metallic baffle was arranged to allow 5 light rays to emerge from a ray box. By adjusting the outer hull of the box, the light rays were made to emerge parallel to each other. In order to verify that the rays were parallel to each other, a ruler was used to compare the distance between the outer rays at various distances from the ray box.

After ensuring that the light rays were parallel to each other, the metallic baffle was readjusted so that only one ray would emerge from the ray box. A white piece of paper was laid flat on the table so that the light ray could be seen clearly across it. Afterwards, a trapezoidal prism was placed in front of the light ray, so that the ray would strike the front interface at an angle of $45.0 \pm 0.5^\circ$. This setup is shown in figure 1.

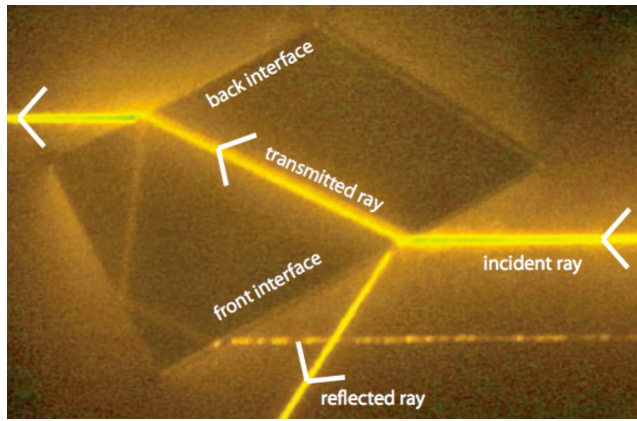


Figure 1: Trapezoidal Prism Setup: This image depicts the setup that was used in this experiment to help verify Snell's Law. The trapezoidal prism was placed so that the front interface created an angle of $45.0 \pm 0.5^\circ$ relative to the incident light ray. The incident, reflected, and transmitted rays at the front and back interfaces were traced on a piece of paper, and a protractor was used to measure the angles. The analysis of these angles could be compared to results based on Snell's Law. (Source: UCLA Physics 4BL Lab Manual, Winter 2016)

After allowing the incident light ray to strike the front interface, the incident ray, reflected ray, and transmitted ray could be clearly seen at the front and back interfaces of the prism. These rays, as well as the normals to the front and back interfaces of the prism, were traced on a piece of paper. The angles of the rays in relation to the normals of the respective prism surfaces were measured through the use of a protractor. The recorded angles are displayed in table 1.

	Incident Angle ($^\circ$)	Reflected Angle ($^\circ$)	Transmitted Angle ($^\circ$)
Front Interface	45.0 ± 0.5	45.0 ± 0.5	28.0 ± 0.5
Back Interface	28.0 ± 0.5	28.0 ± 0.5	45.0 ± 0.5

Table 1: Recorded Angles at Prism Interfaces: This table displays the recorded incident, reflected, and transmitted angles at the front and back interfaces of the trapezoidal prism, which is depicted in image 1. The uncertainty in these values is based on the limited accuracy of the protractor that was used to measure the angles.

2.1.2: Total Internal Reflection

In order to further test the results of Snell's Law, properties of total internal reflection were examined. The trapezoidal prism shown in figure 1 was rearranged so that the single light ray from the ray box would strike the slanted surface first. By rotating the prism, the light ray made to reflect off of one side of the prism, and exit from the interface opposite of the slanted surface.

Total internal reflection was achieved by adjusting the rotation of the prism so that the light at the last interface completely disappeared. The light rays at each surface, as well as the normals to the interfaces of each surface of the prism, were traced on a piece of paper. A protractor was used to

measure the angles of the incident, reflected, and transmitted rays at the front and back interface. The recorded data is shown in table 2.

	Incident Angle (°)	Reflected Angle (°)	Transmitted Angle (°)
Front Interface	18.0 ± 0.5	18.5 ± 0.5	12.0 ± 0.5
Back Interface	42.0 ± 0.5	0.0 ± 0.5	0.0 ± 0.5

Table 2: Total Internal Reflection Data: This table displays the recorded incident, reflected, and transmitted angles at the front and back interfaces of the trapezoidal prism during this portion of the experiment. The incident angle at the back interface provided a measurement of the critical angle for total internal reflection. Snell's Law could be used to calculate a theoretical value for the critical angle, which could be compared to the experimental value.

2.2 Thick Lenses

2.2.1 Focal Length

In the next portion of the experiment, the goal was to examine the focal length of various lenses.

Before doing so, the metallic baffle that was used in previous portions of the lab was rearranged so that three rays emerged from the ray box. Afterwards, a bi-convex lens was placed in front of the rays so that the rays converged at a single point. By moving the lens towards or away from the light source, it was determined that the focal length did not depend on the distance of the lens from the ray box.

After placing the bi-convex lens so that the axis of the lens was normal to the rays, the lens and rays were traced on a sheet of paper. A ruler was used to measure the distance from the center of the lens to the focal point, which gave a measurement of the focal length. This process was repeated for a bi-concave lens, as well as a plano-convex lens. For diverging rays, the rays needed to be traced to the reverse side of the lens in order to find the focal point and focal length. Images of the three lenses that were used are shown in figure 2. The recorded focal length data is displayed in table 3.



Figure 2: Lenses: This image depicts the three lenses that were used in this portion of the experiment. When rays passed through the bi-convex and plano-convex lenses, the rays converged. Conversely, when rays passed through the bi-concave lens, the rays diverged. (Source: UCLA Physics 4BL Lab Manual, Winter 2016)

Lens Type	Bi-convex	Bi-concave	Plano-convex
Focal Length (cm)	5.90 ± 0.05	4.50 ± 0.05	9.50 ± 0.05

Table 3: Focal Lengths of Lenses: This table displays the measured focal length of a bi-convex, bi-concave, and plano-convex lens. This data was found by measuring the distance between the center position and focal point of each lens. The uncertainty in each measurement is based on the limited accuracy of the ruler that was used to measure distances.

2.2.2 Spherical Aberration

In another portion of the experiment, the baffle in front of the ray box was adjusted so that five light rays were allowed to emerge. Afterwards, the plano-convex lens from the previous portion of the lab was placed in front of the rays so that the axis of the lens was normal to the rays. The light rays were observed to converge at two focal points after passing through the lens. After blocking the three middle light rays, it was determined that the outer two rays converged at a point closer to the lens. This was due to the effects of spherical aberration. The positions of the lens and the focal points were marked on a sheet of paper, and a ruler was used to measure the distance between the focal points, as well as the distance from the center of the lens to the midpoint between the focal points. This data could be used to analyze the percent difference between the positions of the focal points. The recorded measurements are displayed in table 4.

Distance from lens to closer focal point (cm)	5.30 ± 0.05
Distance from lens to further focal point (cm)	5.80 ± 0.05
Distance between focal points (cm)	0.50 ± 0.05
Distance from lens to midpoint of focal points (cm)	5.50 ± 0.05

Table 4: Focal Point Measurements: This table displays recorded measurements based on the position of the plano-convex lens in this portion of the experiment, as well as the positions of the two focal points that were produced due to spherical aberration. The percentage of difference between the focal point positions could be used to analyze the effect of spherical aberration on the position of the focal point.

2.2.3 One-Dimensional Magnification

The goal of the next portion of the experiment was to analyze the effects of one-dimensional magnification through the use of lenses. In order to begin, the metallic baffle in front of the ray box was rearranged so that three rays of light would emerge, and the distance between the two furthest rays was measured. After placing a bi-concave lens in front of the light source, the rays were seen to diverge. However, by positioning a plano-convex lens in front of the diverging rays, the rays were made to be parallel once again. This arrangement of lenses caused noticeable magnification of the separation between the light rays, and the distance between the two furthest rays was measured.

Afterwards, the same lenses were placed in reverse order so that demagnification of the spatial separation between the rays occurred. Once again, the distance between the furthest two rays was measured. The data that was gathered through this portion of the experiment is displayed in table 5.

Lens Configuration	No lenses	Bi-concave, then convex	Convex, then bi-concave
Distance between two rays furthest apart (cm)	1.90 ± 0.05	3.80 ± 0.05	0.90 ± 0.05

Table 5: Spatial Separation of Light Rays: This table displays the measured spatial separation between the furthest two light rays after passing through the specified combination of lenses. When light passed through the bi-concave lens and then the convex lens, the spatial separation grew. When the lenses were placed in the reverse order, the spatial separation got smaller. The recorded measurements could be analyzed to see the amounts of magnification and demagnification that were produced by the lens combinations.

2.3 Thin Lens Properties

In the next section of the lab, the focal lengths of various thin lenses were measured. In order to set up the experiment, a single diode laser beam was directed towards a beam splitter, which was set on a magnetic bench at a $45.0 \pm 0.5^\circ$ angle. The uncertainty in the angle is based on the limited accuracy of the protractor that was used to measure it. The thickness of the beam splitter was measured to be 0.90 ± 0.05 cm. The beam splitter reflected two parallel beams, one from the front surface, and one from the back surface. After placing a moveable screen in front of the beams, the distance d between the beams was measured to be 0.80 ± 0.05 cm. The setup is visually displayed in figure 3.

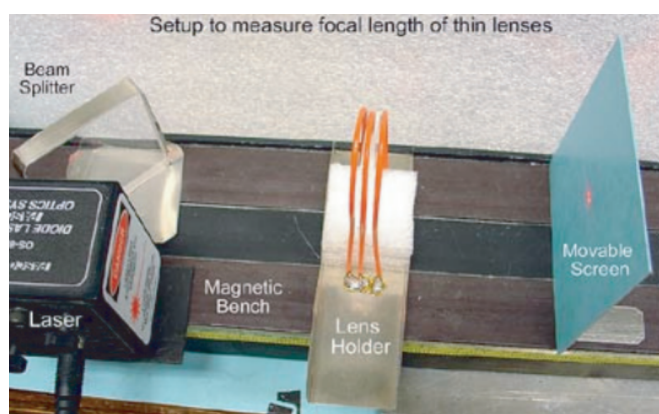


Figure 3: Setup to Determine Focal Length of Thin Lenses: This image displays the experimental setup that was used to measure the focal length of thin lenses. A beam splitter was used to split a single diode laser beam into two beams a distance of 0.80 ± 0.05 cm apart. By placing thin lenses in front of the laser beams, and moving a moveable screen, the beams could be seen to converge when the screen was at a distance equal to the focal length of the lens. (Source: UCLA Physics 4BL Lab Manual, Winter 2016)

After using a lens holder to hold a thin lens in front of the parallel laser beams, a screen was moved towards and away from the lens until the beams converged to a single point. The distance of the screen from the lens at this point was measured to determine the focal length of the lens. This was repeated for two thin lenses separately, for the two thin lenses together, for a 2 cm diameter lens, and for an acrylic sphere. The uncertainty in each measurement was found based on the distance that the moveable screen could be moved without being able to distinguish between the two different beams. The measured focal lengths are displayed in table 6.

	Focal length (cm)
First thin lens l_1	37 ± 4
Second thin lens l_2	15 ± 1
First thin lens l_1 and second thin lens l_2	11 ± 1
2 cm thin lens	16 ± 2
Surface of acrylic sphere	0.5 ± 0.2

Table 6: Focal Lengths of Thin Lenses: This table displays the measured focal lengths of various thin lenses. Each focal length was determined by placing a moveable screen at the focal point (where the laser beams converged), and measuring the distance between the screen and the lenses. The uncertainty in each measurement was based on the distance that the screen could be moved without being able to distinguish between the two beams.

2.4 Image Formation with Lenses

In the last portion of the experiment, a light emitting diode was placed at one end of the magnetic bench, and was powered by a 5 V DC power source. A thin metallic sheet with a millimeter slide located at an aperture was placed next to the diode so that the millimeter slide object was illuminated. By placing the previously used 2 cm lens at a distance o from the millimeter slide object, an image was generated at a distance i on the other side of the lens. This image distance was found by moving a screen towards and away from the lens until the grid lines appeared sharply on the screen. The size I of the image was found by measuring the width of 3 grid squares, and dividing by 3 in order to obtain an average width. The measurements of i , o , and I were found for 5 different lens and screen positions. A visual depiction of the experimental setup is shown in figure 4. The measured data is shown in table 7, and could be used to verify theoretical results based on optics equations.

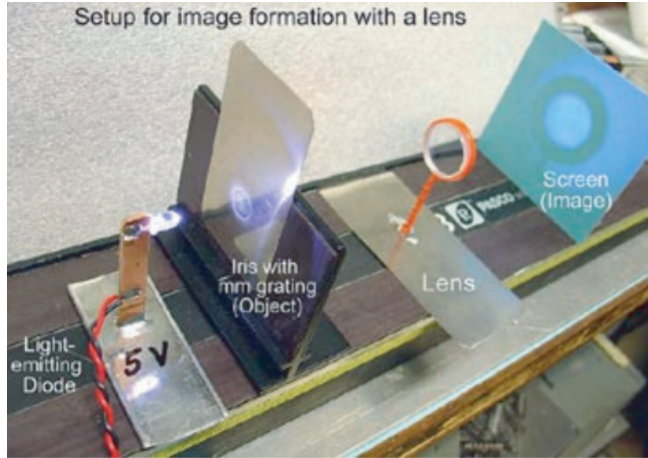


Figure 4: Setup for Image Formation: In this experiment, a light-emitting diode was used to illuminate a millimeter grid that was a distance o from a thin lens. The image distance i , was found determining the distance between the lens and a moveable screen that produced sharp grid lines on the screen. The image size I was determining by finding the width of a grid square in the image. (Source: UCLA Physics 4BL Lab Manual, Winter 2016)

Image distance i (cm)	Object distance o (cm)	Image size I (cm)
34.30 ± 0.05	29.30 ± 0.05	0.113 ± 0.002
33.70 ± 0.05	30.80 ± 0.05	0.107 ± 0.002
32.20 ± 0.05	32.00 ± 0.05	0.100 ± 0.002
30.70 ± 0.05	33.20 ± 0.05	0.090 ± 0.002
29.40 ± 0.05	35.40 ± 0.05	0.083 ± 0.002

Table 7: Image Distance, Object Distance, and Image Size: This table displays the measured image distance i , object distance o , and image size I for multiple setups of the grid object, lens, and screen shown in figure 4. The uncertainty is based on the limited accuracy of the ruler that was used. The uncertainty in image size was calculated based on the propagation of error formula shown in equation 2. This data could be analyzed to see whether or not the experimental results agree with theoretical values and trends.

3. Analysis

3.1 Snell's Law and Total Internal Reflection

3.1.2: Snell's Law

Based on the measured data shown in table 1, the index of refraction n of the trapezoidal prism could be found. This value could be calculated through the use of equation 1, which is based on Snell's Law. For this experiment, the index of refraction of air was accepted to be 1, with negligible uncertainty.

$$n = \frac{n_{air}(\sin\theta_{incident})}{\sin\theta_{transmitted}} \quad (1)$$

$$\sigma_{\bar{F}} = \sqrt{\left(\frac{\partial f}{\partial x}\right)^2 (\sigma_{\bar{x}})^2 + \left(\frac{\partial f}{\partial y}\right)^2 (\sigma_{\bar{y}})^2} \quad (2)$$

Based on equation 1, the index of refraction of the prism was found to be 1.51 ± 0.03 . The uncertainty in this value was found by using the propagation of error formula shown in equation 2.

3.1.2: Total Internal Reflection

Based on the calculated value of the index of refraction n of the prism, the theoretical critical angle of total internal reflection could be found by using equation 3, which was derived from Snell's Law.

$$\theta_{critical} = \sin^{-1} \left(\frac{n_{air}}{n} \right) \quad (3)$$

Based on equation 3, the theoretical critical angle was found to be $41 \pm 1^\circ$. The uncertainty in this value was found by using the propagation of error formula in equation 2. Based on the measured critical angle of 42.0 ± 0.5 , it can be seen that the experimental value agrees with the theoretical value. This positive result helps to verify the results of Snell's Law.

3.2 Thick Lenses

3.2.1 Spherical Aberration

Based on the data shown in table 4, the percentage of difference between the focal point positions relative to the focal point of the central rays could be found by using equation 4.

$$\% \text{ error} = \left| \frac{\text{position 1} - \text{position 2}}{(\text{position 1} + \text{position 2})/2} \right| * 100 \quad (4)$$

In this case, "position 1" was set to be the distance of the focal point created by the central rays, and "position 2" was set to be the distance of the focal point created by the outer rays. Based on the measured focal lengths, the percentage of error was found to be $9 \pm 1\%$. The uncertainty in this value was found by using the propagation of error formula found in equation 2.

3.2.3 One-Dimensional Magnification

The data shown in table 5 could be used to calculate the magnification factor M for the combinations of the bi-concave and plano-convex lenses that were used. The calculations could be made through the use of equation 5.

$$M = \frac{\text{final separation}}{\text{initial separation}} \quad (5)$$

Based on equation 5, the magnification factor when light passed through the plano-convex lens after the bi-concave lens was found to be 2.00 ± 0.06 . Likewise, the magnification factor when the lenses were placed in the reverse order was found to be 0.47 ± 0.03 . The uncertainty in these values was found by using the propagation of error formula found in equation 2.

3.3 Thin Lens Properties

In order to verify the lens combination equation shown in equation 6, the data shown in table 6 could be utilized.

$$\frac{1}{f_{\text{total}}} = \frac{1}{f_1} + \frac{1}{f_2} - \frac{e}{f_1 f_2} \quad (6)$$

Since the distance between the two lenses that were used was very close to 0, equation 6 could be replaced with equation 7.

$$\frac{1}{f_{\text{total}}} = \frac{1}{f_1} + \frac{1}{f_2} \quad (7)$$

If the variable D is set to be equal to $\frac{1}{f}$, then equation 7 could be rewritten as equation 8.

$$D_{\text{total}} = D_1 + D_2 \quad (8)$$

Based on the focal length of 37 ± 4 cm for the first lens, and 15 ± 1 cm for the second lens, the theoretical value of D_{total} was found to be $0.093 \pm 0.008 \text{ cm}^{-1}$. The measured focal length of the combined lenses was 11 ± 1 cm, so the measured value of D_{total} was found to be $0.091 \pm 0.008 \text{ cm}^{-1}$.

The uncertainty in each of these values was found based on the propagation of error formula in equation 2. By comparing the theoretical and experimental values of D_{total} , it could be seen that the values agree with each other based on the error bounds. This positive result helps to verify the lens combination equation.

For the acrylic sphere that was used in the experiment, the focal length f' measured from the surface was found to be 0.5 ± 0.2 cm. This value could be used to calculate the experimental value of the focal length from the center of the sphere based on equation 9.

$$f' = f - \frac{D}{2} \quad (9)$$

Based on equation 9, the focal length f from the center of the acrylic sphere was calculated to be 1.8 ± 0.2 cm. The uncertainty of this value was found by using the propagation of error formula in equation 2. The theoretical value of f could be found by using equation 10, where $n = 1.5$, and $D = 25.4$ mm.

$$f = \frac{nD}{4(n-1)} \quad (10)$$

Based on equation 10, the theoretical value of f was found to be 1.905 cm with negligible uncertainty. By comparing this value to the experimental value of 1.8 ± 0.2 cm, it could be seen that the values agreed with each other based on the given error bounds. This result helps to verify the results of the equations that were used to calculate the focal length of an acrylic sphere.

3.4 Image Formation with Lenses

Based on the 5 image distances and object distances that were displayed in table 7, 5 different experimental values for the focal length of the lens could be calculated. This was done through the use of equation 11. The calculated focal length values are displayed in table 8.

$$\frac{1}{f} = \frac{1}{o} + \frac{1}{i} \quad (11)$$

Measured Focal Lengths
15.80 ± 0.02
16.09 ± 0.02
16.05 ± 0.02
15.95 ± 0.02
16.06 ± 0.02

Table 8: Measured Focal Lengths of Thin Lens: The values in this table show the calculated focal length values for the thin lens that was used in this portion of the experiment, based on equation 11. The uncertainty in each value was found based on the propagation of error formula shown in equation 2.

By taking the average value of the focal lengths shown in table 8, and calculating the uncertainty based on standard deviation, the measured focal length of the lens was found to be 16.0 ± 0.1 cm. The theoretical value for the focal length was taken to be 16 ± 2 cm based on the focal length of the lens shown in table 6. By comparing the experimental and theoretical values, the focal length values can be seen to agree with each other based on the given error bounds. This result helps to verify the results of equation 11.

For each set of data shown in table 7, the magnification factor could be calculated based on equation 12, where the original grid square size $O = 0.1$ cm with negligible uncertainty. The calculated magnification factors are displayed in table 9.

$$M = \frac{I}{o} \quad (12)$$

$$\frac{I}{o} = \frac{i}{o} = \frac{f}{o-f} \quad (13)$$

Position of Object	Magnification Factor	Description
$f < o < 2f$	1.13 ± 0.003	Inverted and magnified
$f < o < 2f$	1.07 ± 0.002	Inverted and magnified
$o = 2f$	1.00 ± 0.002	Inverted and same size
$o > 2f$	0.90 ± 0.002	Inverted and demagnified
$o > 2f$	0.83 ± 0.002	Inverted and demagnified

Table 9: Magnification and Inversion Based on Object Position: The data in this table relates calculated magnification factors to the position of the object that was used. The uncertainty in the calculated values was found by using the propagation of error formula shown in equation 2. By analyzing the data, it can be seen that the magnification and inversion results when $f < o < 2f$, $o = 2f$, and $o > 2f$ followed expected theoretical trends based on equation 13.

Based on the data shown in table 9, it could be seen that varying the object distance in relation to the focal length of the lens resulted in expected magnification and inversion trends. This helps to verify the theoretical results of equation 13.

4. Conclusion

The goal of this lab was to use experimental data to verify equations and theories that are commonly used when dealing with geometric optics. Based on analysis of the first section of the lab, calculations based on light interacting with a trapezoidal prism were found to agree with theoretical values. This helped to verify Snell's Law. In the second portion of the lab, thick lenses were successfully used to analyze properties such as focal length, spherical aberration, and one-dimensional magnification. In the third part of the lab, measured focal lengths of thin lenses were used to successfully verify the lens combination equation, as well as an equation that allowed for the calculation of the focal length at the center of an acrylic sphere. In the final section of the lab, images were formed through the use of a thin lens, and the object distance o , image distance i , and image size I were used to successfully verify the results of theoretical equations relating to image formation. The positive results of this experiment were useful in verifying many theories regarding geometric optics.